PHOTOCONDUCTIVITY OF MACROSCOPIC REDUCED GRAPHENE OXIDE FILMS

James Loomis and Balaji Panchapakesan

Small Systems Laboratory
Department of Mechanical Engineering
University of Louisville
Louisville, KY 40292, USA, b0panc01@louisville.edu

ABSTRACT

This paper reports large photocurrents in air assisted depositions of single layer graphene oxide thin films upon illumination with near-infrared (NIR) light. NIR induced charge carrier generation and subsequent separation at the metal-graphene interface resulted in photocurrent generation. At 100 μV bias, a percent change in current from ~150% (40 mW NIR) to ~1,800% (335 mW NIR) is reported. Such large photocurrent responses result from built-in electric fields and optically generated temperature gradients.

1 INTRODUCTION

Since graphene's 2004 discovery [1], its incredible physical properties including thermal conductivity [2], mechanical strength [3], and quantum hall effect at room temperature [4] have been well documented. Graphene's photonic properties are also quite intriguing, with optical absorption spanning in a broad range from UV to terahertz frequencies [5]. In this paper, we report large photocurrents in airbrushed assemblies of single layer graphene oxide (SLGO). Past reports on graphene photocurrents have demonstrated photoresponse in intrinsic graphene [6], bulk graphite thin films [7], at the interface between single layer and bilayer regions [8], near metallic contacts [9], near edge effects [10, 11], electrostatically doped p-n graphene junctions [12], and more recently gate activated photoresponse on localized regions in graphene p-n junctions [13]. Ultrafast hot carrier effects in graphene that give rise to photocurrents have been hotly debated[14, 15]. It has been shown that a strong electric field near metal-graphene contacts leads to efficient photocurrent generation, resulting in > 30% efficiency for electron-hole separation [16]. Impressive characteristics of graphene photodetection have been well documented in above mentioned studies. However, airbrushed macroscopic assemblies of graphene oxide, where layers are individually deposited to create low density bulk films, have not been explored. These macroscopic films could be of interest in future photoconductivity studies, as small dark current (I_{dark}) values and large near-infrared (NIR) induced photocurrents (I) give rise to high I / I_{off} ratios. Since the number of graphitic layers is known to affect mechanical, photomechanical and thermal properties, exploration of such layered thin films of SLG is of technological interest [17-19]. Samples presented here use simple fabrication techniques, such as air assisted deposition of graphene layers and shadow masks for electrode patterning. These methods do not require lithographic processing, and demonstrate the ability to repeatedly and reliably produce devices with large current responses. Furthermore, effects of varying bias voltages on graphene photodetectors operating in the diffusion and drift regions have not been extensively studied previously.

2 EXPERIMENTAL

Commercially obtained graphene (produced through thermal exfoliation reduction and hydrogen reduction) was purchased from ACS Materials. Graphene oxide was used in original form and not surface modified at any time. Fisherbrand 75 mm × 50 mm glass slides were used as substrates for test sample fabrication. A variable power (500 mW maximum) 808 nm laser, which was collimated to a rectangular spot size of ~ 3 mm × 4 mm, served as the NIR illumination source. Power source profiles were determined using a Newport 1815-C intensity meter. All experiments were conducted in a climate-controlled laboratory. Photocurrent test equipment was operated inside a light-isolated enclosure mounted on an active air suspension table. Cameras inside the test enclosure were continuously monitored to ensure all control and positioning gear operated properly. Custom LabVIEW programs running on a host computer controlled, sequenced, and logged data for all experiments. For more details on experiments please refer to [20].

3 RESULTS AND DISCUSSION

The air assisted deposition technique has been used by our group [21] and others for both large scale dispersions as well as alignment of carbon nanotube

networks [22]. Advantages to air flow deposition include: 1) ability to deposit material on a variety of substrates, 2) flexibility in enabling deposition of conductive material to a range of resistance values, 3) in situ controlled doping of materials with different gases, and 4) geometric straightening of materials such as nanotubes due to airflow generated torque [22]. Because of the honeycomb carbon atom arrangement, during spray deposition graphene can be thought of as a broad two-dimensional (2*D*) mesh being impacted against a substrate by air molecules. Turbulent forces and kinetic energies are imparted on the SLG as it leaves the spray nozzle.

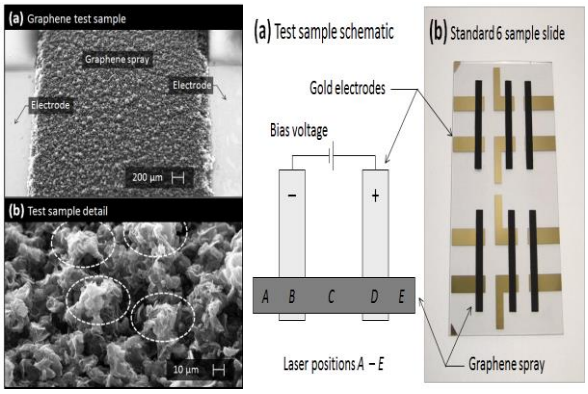

Figure 1: SEM image of graphene spray and test sample schematic.

Figure 1 is a sequence of scanning electron microscope (SEM) images showing detail the bulk graphene morphology resulting from spray fabrication. The first SEM image, Figure 1(a), clearly illustrates sample thickness and electrode placement. Evaluating the topographical surface morphology in greater detail (SEM below), a faint pattern of projecting graphene "balls" becomes visible; several have been circled for clarity. Kinetic energy imparted on the graphene during deposition combined with thermal energy produced from the collisions between graphene layers resulted in this interesting macroscopic morphology. This surface morphology from air assisted deposition is determined by adhesion potential of graphene to the substrate surface and kinetic energy imparted on the graphene from the air spray [22]. Heavier objects, such as stacks of SLG, will have higher kinetic energies and lower contact areas and are therefore less likely to be affected by the substrate adhesion potential. Lighter objects, such as single layers, with lower kinetic energies are more likely to stick to the surface and retain flatter profiles.

Figure 1(b) shows a test sample schematic and standard slide containing 6 individual samples. In order to study position-dependent diffusion dominated photocurrent effects, each test sample was hypothetically divided into 5 NIR illumination "positions". The top view in the sample schematic, Figure 3(a), shows a sequence from *A* to *E* illustrating each of the 5 photocurrent test positions. At positions *A* and *E*, only the graphene "wings" on the outsides of the negative and positive electrodes respectively are illuminated. At positions *B* and *D*, the NIR laser is centered on top of the associated electrode, while at position *C* the NIR spot was placed in the middle of the SLG strip between the electrodes. Prior to NIR illumination, a bias voltage (V_b) was placed across the electrodes (10 µV – 1 V) in order to minimize effects due to Joule heating [23, 24]. The 808 nm NIR laser was collimated to a 3 mm × 4 mm wide rectangle such that it illuminated the entire position of interest, for example the 3 mm × 4 mm section of SLG covering each electrode. Each sample has a set of 4 mm wide gold electrodes separated by a distance of 8 mm, connected by a 3 mm × 26 mm SLG strip. Subsequent photocurrent response experiments were conducted at NIR illumination intensities of 40 mW, 180 mW, and 335 mW. Long term stability of illumination intensities were verified prior to experimentation. Test samples were fabricated on standard glass microscope slides with six test samples per slide, as shown in Figure 3(b). During testing, slides were mounted in a robotic black box testing apparatus in order to measure photocurrent effects of each sample.

Figure 2 shows an overview of typical position dependent NIR-induced photocurrent and associated transients, in this case obtained from a 1.4 kΩ, 400°C annealed sample with a 100 µV bias voltage. Figure 2(a) and (b) illustrate short- and long-term (steady state) position dependent responses to the NIR illumination. Prior to NIR *on*, a dark current exists in the test sample, whose magnitude is a function of bias voltage and sample resistance, following Ohm's law. The high NIR *off* resistance, and consequently small dark current suggests a significant resistance to current flow, possibly due to edge effects [10]. Rather than the similar responses that would be expected, laser illumination of different sample positions of resulted in various changes to the photocurrent. When the laser spot was placed on top of the positive electrode (position *D*), current increased from the I_{dark} value of 70 nA to 1,060 nA, a rise of ~1,400%. Similarly, on the negative electrode (position *B*), a drop in current from 70 nA to –1,200 nA was observed, or a 1,800% decrease. This revealed that current changed direction, even though a forward bias voltage was still being applied. When positions *A* and *E* were illuminated, which are outside the negative and positive electrodes respectfully, it resulted in similar but greatly reduced photoresponses as those obtained when illumination was on positions *B* and *D*. Even more interesting, is when position *C* (center of the SLG test strip) was illuminated, there was minimal induced photocurrent.

Position dependence of photocurrent showed that the positive electrode had the effect of increasing forward current, whereas the negative electrode had the effect of increasing backward current. This suggests built-in potentials exist between the electrode and SLG, this was

also seen in earlier investigations on graphene photoconductivity [7, 8].

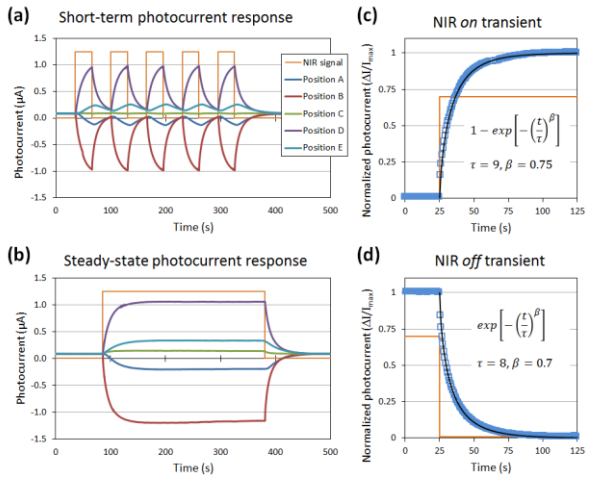

Figure 2: (a) Typical short-term position dependent photocurrent response, (b) Long-term steady-state position dependent photocurrent response, (c – d) NIR *on* and *off* photocurrent transients, respectively.

The differences between our work and others includes investigation into thin film morphology (Figure 1), relationship between annealing temperature and resistance change (Figure 4), demonstration of photocurrent dependence on laser power regardless of resistance (Figure 6), and ability to control device operating region (diffusion versus drift, Figures 8, 9). When NIR illumination is incident to the graphene films, potential barriers between the edges should be overcome due to increases in temperature as well as electric field, thus resulting in such large differences between NIR induced photocurrent and I_{dark}. Upon NIR illumination, graphene absorbs photon energy, resulting in electron-hole pairs or excitons. Without presence of a bias current, these carriers would normally randomly diffuse and recombine in the SLG. However, as they approach the metal-graphene interface hot electrons might have enough energy to cross the Schottky barrier via either tunneling or thermal emission and enter the metal electrode, thus leaving holes in the graphene layers. Once electrons enter the electrodes, a high energy barrier in the reverse direction lowers the probability that they will travel back to the graphene, thereby resulting in charge carrier separation. In real metal-graphene contacts however, defects and surface states exist at the interfaces which affect actual contact band structure. Although past ideal theoretical models illustrate the upward bending of energy bands, a downward bending of energy bands towards the metal could be possible, depending on density and types of surface states [27]. If a downward bending band graph at metal-graphene contacts is assumed, photon generated electrons will naturally favor entering the metal without overcoming energy barriers. This would further result in enhanced charge separation effect, again agreeing with our experimental results.

Figures 2(c) and (d) show NIR *on* and *off* transients respectively. Both were normalized from 0 to 1 using I / I_{max}. In both curves, experimental data fit the exponential form of $I = I_0 exp\left(\frac{-t}{\tau}\right)^{\beta}$, where time constants ($\tau$) are τ ~9 s or light *on* transient and τ ~8 s for light *off*. The slow *on* and *off* response is characteristic of diffusion mediated photoconduction as in past reports [23, 24]. These results can be analyzed using the dynamic model by starting with the continuity equation for minority charge carriers [25]:

$$\frac{d\Delta n}{dt} = -\mu_n E\left(\frac{d\Delta n}{dx}\right) + D_n\left(\frac{d^2\Delta n}{dx^2}\right) - \frac{\Delta n}{\tau_e} + G$$

Where, Δn is non-equilibrium minority carrier concentration, D_n is the diffusion coefficient, τ_e is electron life time, G is non-equilibrium charge carrier generation rate, and E is the electric field. By assuming that carriers were uniformly distributed in the graphene layers and neglecting the small electric field, the equation simplifies to:

$$\frac{d\Delta n}{dt} = -\frac{\Delta n}{\tau_e} + G$$

Then, G can be approximated to ηI, where η is the quantum efficiency and I is the intensity of light.

$$\frac{d\Delta n}{dt} = -\frac{\Delta n}{\tau_e} + \eta I$$

It is seen from the microscopic model for minority charge carrier concentration that steady statephotocurrent is a linear function of the light intensity.

4 CONCLUSIONS

This paper reports large NIR induced photocurrent responses of SLG assemblies fabricated using an air assisted deposition process. This fabrication method produces a low density thin film with unique SLG morphology, akin to clumps of wadded up sheets of paper. As SLG layers impact on top of the substrate and one another during deposition, thermal energy increases their adhesion and contact areas. Although pseudo-3*D* structures were created, NIR *off* currents in the samples were only a few nanoamps. This demonstrated loose morphology and high resistance of layered SLG, with edges of individual layers acting as potential barriers for electron flow. Bias voltages were found to play an integral role in the type of NIR photoresponse. At low bias voltages, diffusion effects dominated, and position

dependency was demonstrated. Photon induced charge carrier generation and subsequent separation at the metal-graphene contact caused changes in photocurrent. Photocurrent exhibited an increase when the positive electrode was illuminated, a decrease when the negative electrode was illuminated, and negligible response when the area between the electrodes was illuminated. At 100 µV bias, a change in photocurrent from ~150% (40 mW NIR) to ~1,800% (335 mW NIR) is reported**.**

REFERENCES

1. Novoselov, K.S., et al., *Electric field effect in atomically thin carbon films.* Science, 2004. **306**(5696): p. 666-669.
2. Balandin, A.A., et al., *Superior thermal conductivity of single-layer graphene.* Nano Letters, 2008. **8**(3): p. 902-907.
3. Lu, Q., M. Arroyo, and R. Huang, *Elastic bending modulus of monolayer graphene.* Journal of Physics D-Applied Physics, 2009. **42**(10).
4. Gusynin, V.P. and S.G. Sharapov, *Unconventional integer quantum Hall effect in graphene.* Physical Review Letters, 2005. **95**(14).
5. Bonaccorso, F., et al., *Graphene photonics and optoelectronics.* Nature Photonics, 2010. **4**(9): p. 611-622.
6. Vasko, F.T. and V. Ryzhii, *Photoconductivity of intrinsic graphene.* Physical Review B, 2008. **77**(19).
7. Lv, X., et al., *Photoconductivity of Bulk-Film-Based Graphene Sheets.* Small, 2009. **5**(14): p. 1682-1687.
8. Xu, X.D., et al., *Photo-Thermoelectric Effect at a Graphene Interface Junction.* Nano Letters, 2010. **10**(2): p. 562-566.
9. Xia, F.N., et al., *Photocurrent Imaging and Efficient Photon Detection in a Graphene Transistor.* Nano Letters, 2009. **9**(3): p. 1039-1044.
10. Lee, E.J.H., et al., *Contact and edge effects in graphene devices.* Nature Nanotechnology, 2008. **3**(8): p. 486-490.
11. Hsu, H. and L.E. Reichl, *Selection rule for the optical absorption of graphene nanoribbons.* Physical Review B, 2007. **76**(4).
12. Rao, G., et al., *Raman and Photocurrent Imaging of Electrical Stress-Induced p-n Junctions in Graphene.* Acs Nano, 2011. **5**(7): p. 5848-5854.
13. Lemme, M.C., et al., *Gate-Activated Photoresponse in a Graphene p-n Junction.* Nano Letters, 2011. **11**(10): p. 4134-4137.
14. Sun, D., et al., *Ultrafast hot-carrier-dominated photocurrent in graphene.* Nature Nanotechnology, 2012. **7**(2): p. 114-118.
15. Song, J.C.W., et al., *Hot Carrier Transport and Photocurrent Response in Graphene.* Nano Letters, 2011. **11**(11): p. 4688-4692.
16. Park, J., Y.H. Ahn, and C. Ruiz-Vargas, *Imaging of Photocurrent Generation and Collection in Single-Layer Graphene.* Nano Letters, 2009. **9**(5): p. 1742-1746.
17. Loomis, J., B. King, and B. Panchapakesan, *Layer Dependent Mechanical Responses of Graphene Composites to Near-Infrared Light.* Applied Physics Letters, 2012. **in press**.
18. Loomis, J., et al., *Graphene nanoplatelet based photomechanical actuators.* Nanotechnology, 2012. **23**(4): p. 045501.
19. Balandin, A.A., et al., *Superior Thermal Conductivity of Single-Layer Graphene.* Nano letters, 2008. **8**(3): p. 902-907.
20. Loomis, J. and B. Panchapakesan, *Large photocurrents in single layer graphene thin films: effects of diffusion and drift.* Nanotechnology, 2012. **23**(26).
21. Shao, N., E. Wickstrom, and B. Panchapakesan, *Nanotube-antibody biosensor arrays for the detection of circulating breast cancer cells.* Nanotechnology, 2008. **19**(46).
22. Hedberg, J., L.F. Dong, and J. Jiao, *Air flow technique for large scale dispersion and alignment of carbon nanotubes on various substrates.* Applied Physics Letters, 2005. **86**(14).
23. Lu, S.X. and B. Panchapakesan, *Photoconductivity in single wall carbon nanotube sheets.* Nanotechnology, 2006. **17**(8): p. 1843-1850.
24. Liu, Y., S. Lu, and B. Panchapakesan, *Alignment enhanced photoconductivity in single wall carbon nanotube films.* Nanotechnology, 2009. **20**(3).
25. Warner, R.M. and B.L. Grung, *Semiconductor Device Electronics*1991: Saunders College Publishing.

ACKNOWLDEGEMENTS

Funding for this work was partially provided by NSF awards: 1202190 and 1233996 for Balaji Panchapakesan